ALMA MATER STUDIORUM
UNIVERSITÀ DI BOLOGNA

ARCHIVIO ISTITUZIONALE
DELLA RICERCA

Alma Mater Studiorum Università di Bologna
Archivio istituzionale della ricerca

Studying physical state of films based on casava starch and/or chitosan by dielectric and thermal properties and effects of pitanga leaf hydroethanolic extract

This is the final peer-reviewed author's accepted manuscript (postprint) of the following publication:

Published Version:
Studying physical state of films based on casava starch and/or chitosan by dielectric and thermal properties and effects of pitanga leaf hydroethanolic extract / Iaccheri E.; Siracusa V.; Ragni L.; De Aguiar Saldanha Pinheiro A.C.; Romani S.; Rocculi P.; Dalla Rosa M.; Sobral P.J.D.A.. - In: JOURNAL OF FOOD ENGINEERING. - ISSN 0260-8774. - ELETTRONICO. - 339:February 2023(2023), pp. 111280.1-111280.25. [10.1016/j.jfoodeng.2022.111280]

Availability:
This version is available at: https://hdl.handle.net/11585/894818 since: 2022-09-30

Published:
DOI: http://doi.org/10.1016/j.jfoodeng.2022.111280

Terms of use:

Some rights reserved. The terms and conditions for the reuse of this version of the manuscript are specified in the publishing policy. For all terms of use and more information see the publisher's website.

This item was downloaded from IRIS Università di Bologna (https://cris.unibo.it/).
When citing, please refer to the published version.

(Article begins on next page)

25 April 2024

This is the final peer-reviewed accepted manuscript of:
Eleonora Iaccheri, Valentina Siracusa, Luigi Ragni, Ana Cristina De Aguiar Saldanha Pinheiro, Santina Romani, Pietro Rocculi, Marco Dalla Rosa, Paulo José do Amaral Sobral
Studying physical state of films based on casava starch and/or chitosan by dielectric and thermal properties and effects of pitanga leaf hydroethanolic extract
which has been published in final form in Journal of Food Engineering Volume 339, February 2023, 111280
The final published version is available online at: https://doi.org/10.1016/j.jfoodeng.2022.111280

Studying physical state of films based on casava starch and/or chitosan by dielectric and thermal properties and effects of pitanga leaf hydroethanolic extract

Eleonora Iaccheri [a], Valentina Siracusa [a, b], Luigi Ragni [a, c], Ana Cristina De Aguiar Saldanha Pinheiro [a], Santina Romani [a, c], Pietro Rocculi [a, c], Marco Dalla Rosa [a, c], Paulo José do Amaral Sobral [a, de, *]

[a] *Department of Agricultural and Food Sciences, Alma Mater Studiorum University of Bologna, Campus of Food Science, Piazza G. Goidanich, 60, 47521, Cesena, Italy*
[b] *Department of Chemical Science, University of Catania, Viale A. Doria 6, 95125, Catania, Italy*
[c] *Interdepartmental Centre for Agri-Food Industrial Research, Alma Mater Studiorum University of Bologna, Campus of Food Science, Via Quinto Bucci 336, 47521, Cesena, Italy*
[d] *Department of Food Engineering, Faculty of Animal Science and Food Engineering, University of São Paulo, Av. Duque de Caxias Norte, 225, 13635-900, Pirassununga, SP, Brazil*
[e] *Food Research Center (FoRC), University of São Paulo, Rua Do Lago, 250, Semi-industrial Building, Block C, 05508-080, São Paulo, SP, Brazil*

ARTICLE INFO

Keywords:
Biopolymers
Sorption isotherms
GAB model
Glass transition
Gordon and taylor model
Dielectric constant

ABSTRACT

Cassava starch (CS) and chitosan (CH) are biopolymers used alone or blended (CS/CH) to produce films, thanks to their excellent film-forming properties. Their main physical properties have been characterized, but their physical and water state have not yet been studied. The objective of this research was to study the water and macromolecular physical state of CS, CH and CS/CH films by DSC and dielectric properties, after sorption isotherms determinations. Biopolymers and obtained films were also analyzed by SEM, FTIR, X-ray diffraction and gas permeability. Dielectric properties of active films containing pitanga leaves hydroethanolic extract were also analyzed. All films presented type II sorption isotherms. Glass transition temperature of films decreased with the increase of moisture content (X_w) following the Gordon and Taylor model. The dielectric constant behaves depending of the monolayer moisture content (X_m): increased linearly as a function of X_w when $X_w > X_m$. For $X_w \leq X_m$, the dielectric constant remained constant. An exponential relationship between α-relaxation and Tg was calculated.

1. Introduction

Films based on biopolymers have been extensively studied because of the environmental concerns related to the use of synthetic plastics. Among the biopolymers, polysaccharides have attracted great attention, thanks to their good film-forming properties. However, these films still have functional property limitations such as poor mechanical and barrier properties, among others (Yusof et al., 2014). An alternative to overcome this problem is to use a mixture of biopolymers (Abd El-Kader and Ragab, 2013; Yusof et al., 2014; Bonilla and Sobral, 2016; Bonilla et al., 2017), thus producing the so-called blends.

Starch and CH are polysaccharides of plant and animal origins, respectively, of high interest in biopolymer film technology. Starch is a polysaccharide formed by two subunits: amylose, usually linear, and amylopectin, which is highly branched (Fennema, 1996). Both are biopolymers whose starting monomer is glucose. Particularly, CS, which has excellent film-forming properties, is a raw material widely produced on several continents and at a relatively low cost (Bergo et al., 2008, 2010, 2012). Indeed, CS can form transparent and flexible films without any previous chemical treatment, or even without plasticizer addition (Vicentini et al., 2005).

CH, in turn, despite being more expensive and more restricted in production, has attracted attention also for its good film-forming property, but above all for its intrinsic antimicrobial behavior (Bonilla and Sobral, 2016). CH is a partially deacetylated biopolymer of acetyl glucosamine, obtained after the alkaline N-deacetylation of chitin (Hadi et

* Corresponding author. Department of Agricultural and Food Sciences, *Alma Mater Studiorum* University of Bologna, Campus of Food Science, Piazza G. Goidanich, 60, 47521, Cesena, Italy.
E-mail address: pjsobral@usp.br (P.J.d.A. Sobral).

© 2022 Elsevier. This manuscript version is made available under the Creative Commons Attribution-NonCommercial-NoDerivs (CC BY-NC-ND) 4.0 International License (https://creativecommons.org/licenses/by-nc-nd/4.0)

Note: Low-resolution images were used to create this PDF. The original images will be used in the final composition.

al., 2020). It is insoluble in water, but it became soluble at pH below 6.5, being a positive polyelectrolyte due to the presence of $–NH_3^+$ functional groups. Whereas starch has only one functional group (-OH), CH has two kind of functional groups (-OH and $–NH_3^+$) (Fahmy et al., 2020; Hadi et al., 2020). Both biopolymers are commercialized as partially crystalline powders (Bergo et al., 2012; Fahmy et al., 2020).

Recently, Chakravartula et al. (2020) developed active films based on blends of these two biopolymers (CS:CH 2:1 ratio). These authors studied their main physical and functional properties, but lacked to determine gas permeability and to study them at structural-molecular level. In this sense, differential scanning calorimetry (DSC) and dielectric spectroscopy (DS) techniques have been used to study the molecular dynamic in biopolymeric films (Lazaridou and Biliaderis, 2002; Abd El-Kader and Ragab, 2013).

DSC is a well-known technique that allow to assess the thermal properties of materials, such as the glass transition temperature (Tg) (López-Angulo et al., 2020). Several authors reported the Tg values of films based on CS (Famá et al., 2006; Bergo et al., 2008; Souza et al., 2012) and on CH alone (Dong et al., 2004) or blended with gelatin (Bonilla et al., 2017), and even blended with synthetic polymers (El Sayed and Mohamad, 2018; Fahmy et al., 2020). It is very important to study this property because frequently it defines a state of relative high stability and also because a small change in temperature in the proximity of Tg could result in important changes in mechanical and dielectric properties of films, among others physical properties (Lazaridou and Biliaderis, 2002).

During DS analysis, with increasing frequency, the dielectric constant (ε′) decreases and the dielectric loss (ε") shows a peak due to the delay in the dipole moment, a phenomenon called dielectric relaxation (Iwamoto et al., 1999). Dielectric relaxation is the decrease in the ε′, and the maximum value of the ε". The phenomenon of dielectric relaxation, analyzed at different temperatures, has been associated by several researchers with the glass transition phenomenon, studied by DSC, as discussed above (Bergo et al., 2008, 2010). Particularly, these phenomena can affect the physical properties of films, including their gas barrier properties (Siracusa, 2012).

Thus, the dielectric properties of a material can provide valuable information concerning the mobility of polymers chemical chains, bearing dipolar regions or dipolar side groups (Abd El-Kader and Ragab, 2013). DS allows investigating the penetration of water through films and its role as film plasticizing agent (Bergo et al., 2012). The dielectric properties (e.g., ε′ and ε") were especially sensitive to moisture in gelatin films (Bergo et al., 2013) and CS films (Bergo et al., 2012), a phenomenon that can be explained based on the way water penetrates the film matrix (Bergo et al., 2012). Valencia et al. (2014) observed that the conductivity, another dielectric property, increased with the concentration of glycerol in potato starch films, mainly due to the movement of ions that occurs in a separate second phase composed mainly of water and glycerol. Bergo et al. (2012) observed that ε' of CS films was strongly dependent on the moisture content, showing a constant value and a linear region, which were attributed to the domain of bound and free water in the film, respectively.

The objective of this work was to study the water and macromolecular physical state of different films (CS, CH and its blend) assessing their thermal properties by DSC and their dielectric properties by DS. Films under analyses were pre-conditioned at different relative humidity allowing sorption isotherms determination. Moreover, this study was complemented by analysis carried out by scanning electron microscopy (SEM), Fourier-transformed infrared (FTIR) and X-ray diffraction (XRD) spectroscopies of films and their biopolymers and also by the evaluation of the oxygen and carbon dioxide permeability of some films. Active films were produced by incorporating pitanga leaves hydroethanolic extract into CS/CF film formulation and were analyzed by DS to verify the effect of this extract on water and macromolecule physical states in films.

2. Material and methods

2.1. Material

CS was purchased from Amalfi Ind. and Com. de Alimentos Ltda (Cianorte, Paraná, Brazil), CH from shrimp shells (low viscosity and ≥75% diacetyled) was purchased from Sigma Aldrich, Co. (Germany). Acetic acid (≥99.8%) was purchased from Sigma Aldrich, Co. (Steinheim, Germany) and glycerol (anhydrous) was purchased from Merck KGaA (Darmstadt, Germany).

Pitanga leaves hydroethanolic extract (PLHE) was produced according to Tessaro et al. (2021). Briefly, Pitanga leaves, collected at Pirassununga (21°59′46″S, 47°25′36″W, São Paulo, Brazil), were dried at 30 °C, crushed, and sieved in a 48-mesh sieve. This material was then dispersed in 60% hydroethanolic solution (1 g leaves powder/10 mL solvent), treated by ultrasound (1440 DA, Odontobras, Brazil) at room temperature for 40 min, and heated in a magnetic heater (AA-2050, Gehaka, Brazil) at 80 °C for 30 min. After that, the dispersion was filtered with filter paper (Whatman Nº:1). The filtered extract was evaporated (Rotary vacuum evaporator TE-211, Tecnal, Brazil) at 40 °C for 4 h, freeze-dried in a freeze dryer (FD 1.0–60, Heto, Germany) and stored in the dark. Finally, to produce active films, this freeze-dried powder was suspended in distilled water (1 g/10 mL distilled water). PLHE has been characterized by Lorenzo et al. (2018) using UHPLC-ESI/QTOF chromatography to be composted by 35.13 g/kg of phenolic compounds, being around 88% ascribed to tyrosols and other phenolics together with hydroxycinnamic acids.

2.2. Biopolymers characterizations

CS, CH, and CS/CH (2:1) blends were analyzed by scanning electron microscopy (SEM), Fourier-transform infrared spectroscopy (FTIR), and X-ray diffraction spectroscopy.

2.2.1. Scanning electron microscopy (SEM)

Samples were analyzed by SEM using a HITACHI Tabletop Microscope TM3000 (Hitachi Ltd, Tokyo, Japan). Samples were mounted on copper stubs and analyzed with an accelerating voltage of 5 kV, without any previous preparation (Valencia et al., 2016).

2.2.2. Fourier transform infrared spectroscopy (FTIR)

FTIR spectra of samples were obtained using an FTIR spectrophotometer (PerkinElmer Spectrum One, Stuttgart, Germany) from the wavenumber 4000 to 550 cm^{-1} with a resolution of 4 cm^{-1}.32 scans were done using the Universal Attenuator Total Reflectance (UATR) accessory (Tessaro et al., 2021). The FTIR spectra were taken in transmittance mode.

2.2.3. X-ray diffraction (XRD) spectroscopy

X-ray diffractograms of samples were obtained using an X-ray diffractometer (AXS Analytical X-ray Systems Siemens D 5005, Germany), operating at 40 kV and 40 mA (Cu Kα 1, $\lambda = 1.54056$ Å radiation). Spectra were recorded at 25 °C between the angles $2\theta = 2$ and 50° at a rate of 2°/min. (Valencia et al., 2018).

2.3. Production of films

The films were produced by film casting procedure, according to Chakravartula et al. (2020), with some modifications. CS film-forming solution (FFS) was prepared by dispersing 2% of CS in distilled water, by heating at 90 °C for 30 min under mixing. CH FFS was prepared with 2% of CH in 1% acetic acid aqueous solution, at 40 °C, under continuous mixing (Bonilla and Sobral, 2016). In both cases, 25 g of glycerol/100 g of biopolymers was added, as a plasticizer. To produce films

based on blends of CS/CH, the respective solutions were mixed in a CS:CH ratio of 2:1 according to Chakravartula et al. (2020).

Finally, to produce active film, 2.25 g of PLHE solution/100 g of FFS was added to previously prepared CS/CH solution, considering enough to attain the objective of this word (Chakravartula et al., 2020). All these solutions were poured into plexi plates in convenient amounts to guarantee 2.4 g of dry solids/plate and dehydrated in an air circulation oven, at 30 °C for 16–24 h (Tapia-Blácido et al., 2013). Films thickness remained around 0.184 ± 0.012 mm, measured using a Sample Thickness Tester (DMG Device, Model MarCator 1086 type, Mahr GmbH, Esslingen, Germany). The moisture content of films was determined only after conditioning.

2.4. Films characterizations

The main characterizations carried out in this study were thermal (by DSC) and dielectric properties (by DS), and sorption isotherms determinations. Nevertheless, films were also submitted to SEM, FTIR and DRX analyzes as described in 2.2.1, 2.2.2 and 2.2.3, respectively. Cross-sections of film samples were analyzed after sample cryo-fracturation after quench cooling in liquid nitrogen.

Moreover, passive and active (containing PLHE) CS/CH films were analyzed for determination of the barrier property to O_2 and CO_2 through a manometric method using a Permeance Testing device (type GDP-C, Brugger Feinmechanik GmbH, Germany), following the Gas Permeability Testing Manual. Film sample were tested under a gas stream of 100 cm^3/min, 0% RH (food grade gases) at 23 °C, controlled with an external thermostat bath (HAAKE-Circulator DC10-K15 type, ThermoFisher Scientific, Waltham, MA, USA). The gas permeability was determined considering the increase in pressure in relation to time and volume of the device. Each measurement was performed in triplicate.

2.4.1. Sorption isotherms

Sorption isotherms were determined for the different films by using static isopiestic methods using saturated salt solution, at 22 ± 1 °C (Labuza et al., 1972). Static desiccators (Kartell ®) with saturated salt solutions (LiCl, $KC_2H_3O_2$, $MgCl_2$, K_2CO_3, NaBr, and NaCl) were used to produce different relative humidity, ranging from 11 to 75%. Three batches and three different samples for each film (3–5 g), weighted in an analytical balance (±0.001 g), were employed for every water activity (a_w) level. The thermodynamic equilibrium was evaluated by weighting samples three consecutive times to reach a steady weight with $\Delta_{weight} < 0.005$ g for about 4 weeks, at least. Equilibrium moisture content was determined gravimetrically by drying at 105 °C until steady weight (Bonilla and Sobral, 2016). All these analyses were conducted at least in triplicates.

The GAB (Guggenheim, Anderson, & de Boer) model (Eq. (1)) is one of the most popular mathematical models able to describe sorption behavior in a water activity ranges from 0.05 to 0.95 (Barbosa-Canovas et al., 2020).

$$X_w = \frac{X_m C_{GAB} K_{GAB} a_w}{\left(1 - K_{GAB}\, a_w\right)\left(1 + \left(C_{GAB} - 1\right)\, K_{GAB}\, a_w\right)} \quad (1)$$

where X_w is the equilibrium moisture content (kg/kg dry basis), Xm is the monolayer moisture content (kg/kg dry basis) and C_{GAB} and K_{GAB} are the GAB model constants related to enthalpic and entropic contribution of sorption heat, respectively.

The GAB model (Eq. (1)) was fitted to experimental X_w *vs* a_W data by non-linear regression (Marquart algorithm) using the Statistica® 7.0 (Stat-Soft Inc., USA), with a level of confidence of 95%. Coefficients of determination, R^2 (level of confidence 95%), related Root Mean Square Error (RMSE), and mean relative percentage deviation (E, %) were used to evaluate the goodness of model estimation.

2.4.2. Differential scanning calorimetry (DSC)

Tg of films was determined by using DSC Q20 (TA Instrument, Germany) equipped with a cooling subunit System 90 (TA Instrument, Germany), according to Iaccheri et al. (2020). Two calibrations were performed before analyses. The same heating rate set in the programmed temperature was applied under a dry nitrogen gas flux (50 mL/min) to perform the first calibration. Then, the heat of fusion of Indium (ΔH = 28.71 J/g) was measured to calibrate heat flow. Each sample of about 3 mg was analyzed in triplicate. For this, sample was placed in a 50 μl hermetic aluminum pan, weighed and then loaded with an autosampler into the DSC instrument at room temperature. An empty pan was used as reference.

For the analysis, samples were equilibrated at 22 °C for 20 min, and then cool-heat cycles were applied from −80 to 200 °C at 20 °C/min. The automatic tool of the TA-Universal analyzer (TA Instrument, Germany) software was used to evaluate variations of heat flux (W/m^2) in terms of peaks (such as melting peak) and step changes of the baseline, as Tg event, calculated as its midpoint temperature.

2.4.3. Dielectric properties

Dielectric properties were assessed at 22 °C, in triplicate, in a wide radiofrequency range from 250 MHz to 3 GHz. Data acquisitions were carried out by using an open-ended coaxial probe (DAKS-3.5 probe, Speag) connected to an R-140 VNA (Vector Network Analyzer, Copper Mountains) and interfaced via USB to a computer. A dedicated software (DAK Software Installer 2.6.1.7) was used for calibration and acquisition. The device was calibrated by using the company calibration kit (Speag DAK-3.5/1.2 Shorting Block, Metallic Strip Sets, and 0.6 L of simulating liquid with intermediate values of dielectric constant, and loss factor) accounting for open, short, and load assessment. The coaxial probe was fixed with a stainless-steel support to avoid possible changes due to cable movements, and samples were kept in contact with the probe by an elevation platform (Fig. 1). The dielectric constant (ε'), the loss factor (ε"), and the conductivity (σ, S/m) of the different samples were directly recorded by DAK software.

3. Results and discussions

3.1. Biopolymers characterizations

3.1.1. Scanning electron microscopy (SEM)

The scanning electron micrographies allowed to observe that CS granules (Fig. 2A) were uniformly smooth, without scratches, and with a truncated form, typical of CS granules (Valencia et al., 2016), whereas

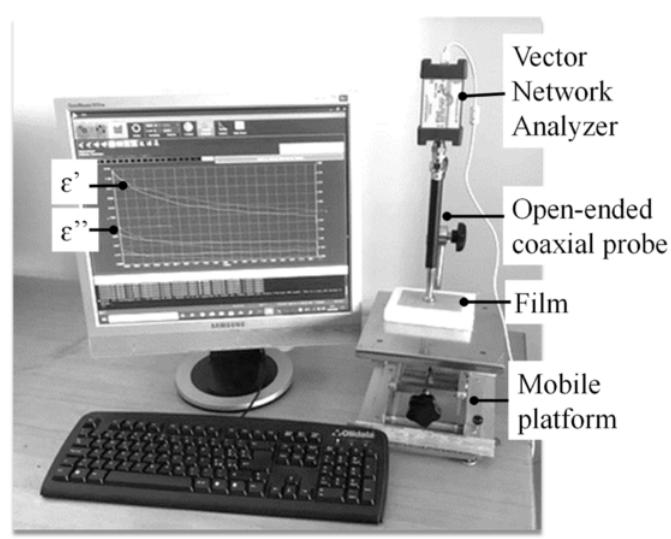

Fig. 1. Layout of the instrumental chain for dielectric properties assessment.

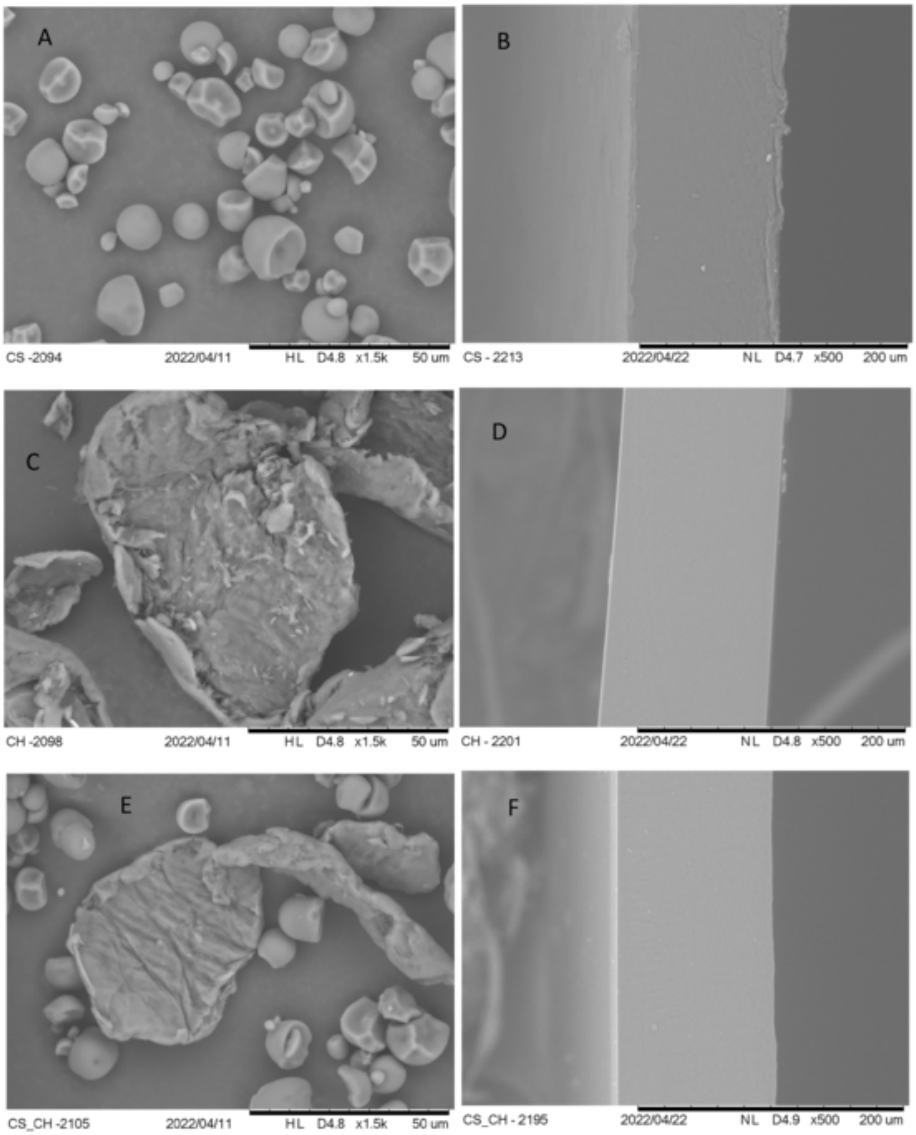

Fig. 2. Scanning electron micrographs of raw material (A,C,E) and its films (B,D,F): cassava starch (A,B), chitosan (C,D) and blend of cassava starch:chitosan (2:1) (E,F). Magnifications: 1500× (left) and 500x (right).

CH powder (Fig. 2C) was formed by rugous unevenly broken and fibrously structures, in some cases, appearing as scales. The mixing of these powders did not change their morphologies (Fig. 2E): CS/CH mix showed both the CS and CH granules without mixing or changing their shape properties alone. It was possible to note that CS and CH particles presented a broad size distribution, varying approximately between ~5 and ~16 μm and ~8 and ~300 μm, respectively.

3.1.2. Fourier transform infrared spectroscopy (FTIR)

FTIR spectrum of CS (Fig. 3A) showed a band centered at 3296 cm^{-1} which corresponds to symmetrical and asymmetrical stretching of –OH bonds, nevertheless, this signal can also be due to the presence of water molecules into samples (Pavia et al., 2001). The next band, observed at 2932 cm^{-1}, was associated to the asymmetrical stretching of –CH bonds, and at 1635 cm^{-1}, a band corresponding to the vibration of –OH groups, appeared (Pavia et al., 2001). Moreover, in the starch fingerprint, it is possible to note a band at 1149 cm^{-1}, corresponding to the CO bonds stretching, and another band at 997 cm^{-1}, which is typical of intramolecular hydrogen bonding of the hydroxyl group at C-6, and distinctive of biomaterials partially crystalline (Vicentini et al., 2005). A symmetric elongation of C–O–C groups was observed at 929 and 860 cm^{-1} (Vicentini et al., 2005).

Analyzing the FTIR spectrum of CH (Fig. 3A), it was possible also to identify the band at 3354 cm^{-1} associated to stretching vibrations of O–H and N–H groups and O–H/N–H interacting with the oxygen of C═O group, followed by a band at 2875 cm^{-1} associated to the asymmetrical stretching of –CH (Fahmy et al., 2020). Some signals associated to N-acetyl groups were identified: 1650 cm^{-1}, corresponding to the C═O stretching of amide I, and 1585 cm^{-1}, associated to N–H of amide II (Lertsutthiwong et al., 2012). The band at 1375 cm^{-1} was associated to the vibrations of the –OH group of the primary alcoholic group (Bonilla and Sobral, 2016). The bands observed at 1418 and 1316 cm^{-1} corresponded to $–CH_2$ bonding of methylene groups and methyl groups, respectively. The bands at 1150, 1060, 1021 and 895 cm^{-1} can be attributed to glycosidic linkages and the stretching of C–O–C of the polysaccharide chain (Lertsutthiwong et al., 2012; Duran-Baron et al., 2017; Fahmy et al., 2020). Moreover, the band at 894 cm^{-1} corresponded to the C–H curve out of the ring plan of monosaccharides (Bonilla and Sobral, 2016).

Finally, the FTIR spectrum (Fig. 3A) of mixed biopolymers (CS:CH 2:1) presented the same signals of the pure products spectra, as de-

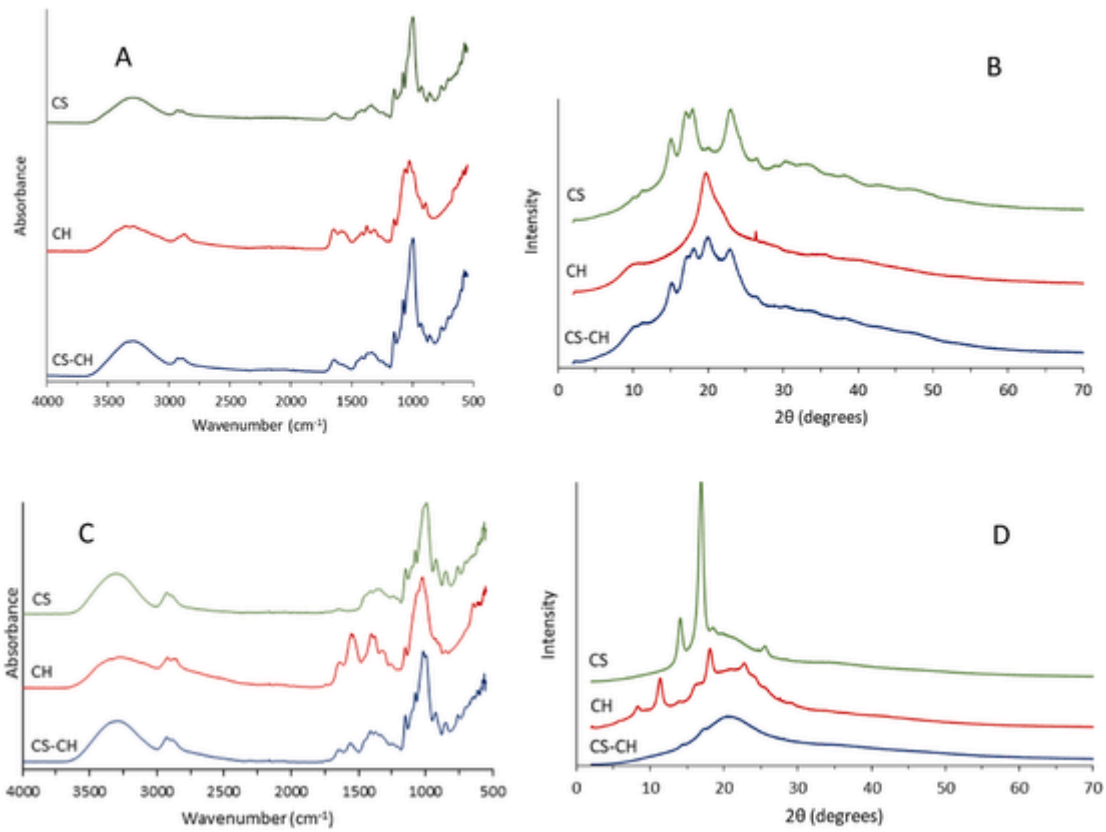

Fig. 3. Fourier-transformed infrared spectra (A,C) and X-ray spectra (B,D) of raw material (A,B) and its films (C,D): CS – cassava starch, CH – chitosan, and CS-CH – blend of CS/CH.

scribed above. This could be expected because this product is a single blend. These results are important as the control to the respective films spectra, in order to understand possible interactions occurring during films processing.

3.1.3. *X-ray diffraction (XRD) spectroscopy*

The XRD spectra of raw material are presented in Fig. 3B. It can be observed that CS spectrum exhibited a diffraction pattern of A-type crystalline, typical of starch originated from plant roots (Valencia et al., 2014, 2016), with a crystallinity of 17%. CS presented crystalline peaks at $2\theta = 15^\circ$ and 23°, and an unresolved doublet at $2\theta = 17^\circ$ and 18°, over a big and broad peak corresponding to the amorphous portion of this material. These results were similar to those determined by Valencia et al. (2016), on CS, and by Abd El-Kader and Ragab (2013) on maize starch.

On another side, CH spectrum (Fig. 3B) presented two subtill peaks at $2\theta = 11^\circ$ and 26°, and a more pronounced one at $2\theta = 20^\circ$, with a crystallinity of 12%. These results are quite different from those ($2\theta = 9^\circ$, 12°, 19°, and 23°) determined by El Sayed and Mohamad (2018). Lertsutthiwong et al. (2012) analyzed a sample of CH between $2\theta = 3^\circ$ and 15° and observed a peak at $2\theta = 11^\circ$, similar to the first peak observed in this study (Fig. 3B). The XRD spectrum of the CS/CH blend characterized by all peaks from each biopolymer, that is $2\theta = 15^\circ$, 17°, 18°, and 23° for CS, and $2\theta = 11^\circ$, 20°, and 26° for CH, and an intermediate crystallinity of 14%. No XRD results on CS/CH blends were found in the literature.

3.2. *Films characterizations*

3.2.1. *Scanning electron microscopy*

The results of SEM allowed to observe that all films presented a very homogeneous microstructure (Fig. 2 B,D,F), without any relation with their raw material (Fig. 2 A,C,E), meaning that the biopolymers solubilization process was completed and that biopolymers were structurally compatible. This is important to produce films with enhanced functional and physical properties. The microstructure of these films was more homogeneous than the oriented structure observed by Silva-Weiss et al. (2013), working with similar films, and were similar to those observed by Bonilla and Sobral (2016) and Duran-Baron et al. (2017).

3.2.2. *Fourier transform infrared spectroscopy (FTIR)*

Passive films contain, besides biopolymers, the glycerol, a plasticizer necessary to produce a flexible material. Eventual interactions between biopolymers and glycerol, and even between CS and CH for films based on this blend, can occur in the form of hydrogen bonds which can be manifested in FTIR spectra as shifts in respective bands (Fahmy et al., 2020). Then, FTIR spectra of CS films (Fig. 3 C) showed these effects for bands at 2925 and 1644 cm^{-1}, which shifted, respectively, from 2932 to 1635 cm^{-1} of CS (Fig. 3 A), as a consequence of effect of glycerol on the asymmetrical stretching of –CH bonds, and on the vibration of –OH groups (Pavia et al., 2001). In the starch fingerprint, shifts between CS (Fig. 3 A) and CS films (Fig. 3 C) spectra were also observed in the bands from 929 to 924 cm^{-1} and from 860 to 848 cm^{-1}, as a consequence of the presence of glycerol placed between the starch macromolecular chains which could affect the symmetric elongation of C–O–C groups into starch macromolecules (Bergo et al., 2010, 2012). No important changes in other bands of this regions implied that the glycerol didn't affect the crystallinity of this material (Vicentini et al., 2005).

The CH film FTIR spectra (Fig. 3 C) showed more important changes as compared with those of CH powder (Fig. 3 A). The band at 3354 cm^{-1} shifted to 3276 cm^{-1} due to possible interaction bonds between the O–H groups of glycerol with O–H and N–H groups and between these groups and the oxygen of C═O group of CH (Fahmy et al.,

2020). After that, a shift was also observed in the band at 2875 to 2870 cm^{-1} followed by the appearing of a band at 2922 cm^{-1}, not visible in –CH (Fig. 3 A), also associated to the asymmetrical stretching of –CH (Fahmy et al., 2020), probably due to the plasticizer effect of the glycerol (Bergo et al., 2010). Shifts were also observed in the signals associated to N-acetyl groups: from 1650 to 1640 cm^{-1} and from 1585 to 1557 cm^{-1}, as a consequence of the effect of glycerol on the C═O stretching of amide I, and on N–H of amide II, respectively (Lertsutthiwong et al., 2012). Obviously, the band linked to the vibrations of –OH group of the primary alcoholic group of –CH was also affected and then shifted from 1375 to 1379 cm^{-1} (Bonilla and Sobral, 2016). The presence of glycerol in the film also affected the bands observed at 1418 and 1316 cm^{-1} in CH which shifted to 1404 and 1319 cm^{-1}, respectively, but appearing a new band at 1379 cm^{-1}, all corresponding to $–CH_2$ bonding of methylene groups and methyl groups, respectively.

Overall, the CS/CH film FTIR spectra (Fig. 3 C) showed signals from both biopolymer spectra (Fig. 3 A), with some slightly changes. When film produced using CS or CH and glycerol were analyzed, the band associated to interactions bonds between the O–H groups of glycerol and starch chains with O–H and N–H and C═O groups of CH appeared at 3290 cm^{-1} (Fahmy et al., 2020). With the presence of the glycerol in biopolymer matrix, more –OH groups were available for starch-glycerol and CH-glycerol interactions, thus affecting this band (Yusof et al., 2014). Also, a slight change was visible with bands at 2877 and 2925 cm^{-1}, being that this last signal was not visible neither in the biopolymer (Fig. 3 A) nor for CH film (Fig. 3C), but was observed by Chakravartula et al. (2020), analyzing films based on blends of CS/CH. In the domain of amides groups, change was observed only for the C═O stretching of amide I with a band at 1646 cm^{-1}, which suggests a good interaction between film constituents (Fahmy et al., 2020). The band linked to the vibrations of –OH group of the primary alcoholic group of –CH came back to 1372 cm^{-1} similar to that of the –CH films spectrum (Bonilla and Sobral, 2016). The bands observed at 1409, 1336, and 1373 cm^{-1}, corresponding to $–CH_2$ bonding of methylene groups and methyl groups, underwent a little shift. A characteristic peak at 1151 cm^{-1}, assigned to C–O–C in glycosidic, appeared in spectra of both films with CS, indicating that the glycosidic chain length was not modified by film processing nor by the glycerol presence (Silva-Weiss et al., 2013).

3.2.3. X-ray diffraction (XRD) spectroscopy

Despite the gelatinization of starch during the film processing, CS film had a semicrystalline character, with four peaks in its XRD spectrum (Fig. 3 D), but not necessarily at the same position as CS powder (Fig. 3 B), with a crystallinity of 20%. Only peaks at $2\theta = 17°$ and 18° appeared in both spectra, nevertheless, peaks at $2\theta = 14°$ and 26° were observed only for CS film (Fig. 3 D). Valencia et al. (2018) produced nanocomposites based on CS and montmorillonite and observed that these films were amorphous, but Pelissari et al. (2013) on films based on plantain banana starch observed the same peaks in both spectra of starch and its films. The crystallinity of CS films was probably due to retrogradation which occurred during drying and conditioning process. More generally, the crystallinity of starch-based films can be influenced by the amylose/amylopectin ratio, the degree of branching and the length of the amylopectin outer chains, the starch source, the conditions of the drying process, and the final moisture content of the samples (Pelissari et al., 2013). Crystallinity can affect some properties of films, mainly their mechanical and barrier properties.

On another side, XRD spectrum of CH film (Fig. 3 D) presented a higher number of peaks/shoulders as compared with CH powder spectrum (Fig. 3 B), and a lower crystallinity (8%). Only the peak at $2\theta = 11°$ appeared in both spectra. Peaks which appeared at $2\theta = 20$ and 26° in the CH powder spectrum were shifted to $2\theta = 18°$ and 23°, respectively, and news peaks appeared at $2\theta = 8°$ and 14°, although very subtill, in the CH film spectrum. These peaks occurring in low values of 2θ were observed in both CH and film based on CH blended with polyvinylpyrrolidone (El Sayed and Mohamad, 2018). The CS/CH film spectrum (Fig. 3 D) showed that this material was almost completely amorphous, with a crystallinity of 7%.

Passive and active CS/CH films presented the following results for gas permeability: 1.12 ± 0.03 and 1.15 ± 0.01 $cm^3/cm^2 day.bar$ for O_2, respectively, and 0.27 ± 0.03 and 0.40 ± 0.00 $cm^3/cm^2 day.bar$ for CO_2, respectively. These values were very lower than those determined by Siracusa et al. (2018) on films based on sodium alginate and/or pectin (110–148 and 96–144 $cm^3/cm^2 day.bar$ for O_2 and CO_2, respectively), and then those determined by Souza et al. (2012) on CS films (42–424 $cm^3/cm^2 day.bar$). Moreover, it was observed that the PLHE provoked an increase on both permeabilities, explained by its effect on the physical state of films (described in 3.2.2 section).

3.2.4. Sorption isotherms

Sorption isotherms of CS, CH, and CS/CH films were presented in Fig. 4, where it is possible to observe that these curves were sigmoidal. This sigmodal behavior has been also observed by others authors for films based on CS (Mali et al., 2005; Bergo et al., 2012; Teodoro et al., 2015), CH (Wiles et al., 2000; Aguirre-Loredo et al., 2017; Monte et al., 2018) and in films produced by blowing-extrusion with a blend of CS/CH incorporated with oregano essential oil (OEO) (Pelissari et al., 2011), at the same temperature of this study. The observed sorption isotherm behavior is typical of products rich in macromolecules such as proteins and polysaccharides (Tapia-Blácido et al., 2013).

Table 1 reports the GAB parameters describing the sorption profiles of films. GAB model revealed a good determination coefficient ($R^2 > 0.98$) and RMSE→0 confirming a good estimation of the model. The X_m was lower (6.2%) for CS (Fig. 4 A), higher (15.9%) for CH (Fig. 4 B) and intermediary (7.9%) for CS/CH (Fig. 4 C) blend films (Table 1), corresponding to monolayer a_w equal to 0.11, 0.33 and 0.18, respectively. This means that CH film had more amount of active site to be recovered by the water molecules, also due to the presence of $–NH_3^+$ in that macromolecule. Moreover, the low value of X_m for CS film can also be due to its high crystallinity (Fig. 3 D), considering that water absorption occurs into amorphous portion. The intermediary position of X_m for CS/CH blend film was due to an additive effect of both biopolymers. X_m is the optimal moisture content for dried food storage, in which the material has maximum stability in relation to oxidation reactions (Labuza et al., 1972). So, for active films, in a technological point of view, this condition is very important to guarantee the maximum stability of bioactive compounds during storage before application as food packaging.

The values of X_m determined in this study (Table 1) were similar to those calculated (at 25 °C) by several authors: CS, 8% (Teodoro et al., 2015), CH, 10.2% (Aguirre-Loredo et al., 2017) and CS/CH blend films with OEO, 5.7–8.9% (Pelissari et al., 2011). Moreover, Monte et al. (2018) calculated $X_m = 20$ and 18% for films based on CH, at 20 and 30 °C, respectively, and Mali et al. (2005) calculated $X_m = 5.2$ and 9.1% for CS films with 20 and 40% of glycerol, respectively, at 25 °C.

Accordingly, CH film (Fig. 4 B) had a huge portion of water bound to the monolayer, but also more water bound to the multilayer, while CS film (Fig. 4 A) shown more free water, and the blend presented an intermediate behavior (Fig. 4 C). Actually, CH film had the highest bound water content confirming that water was bound in different way, showing the most stable profile regarding sorption behavior.

C_{GAB} is a measure of the strength of binding of water to the primary binding sites, i.e., forming a water molecules monolayer, and K_{GAB} is associated with water-water biding in the multilayer, which was formed over the monolayer (Blahovec and Yanniotis, 2008). According to Blahovec and Yanniotis (2008), for sigmoidal shape sorption isotherms corresponding to the II Type of Brunauer's classification,

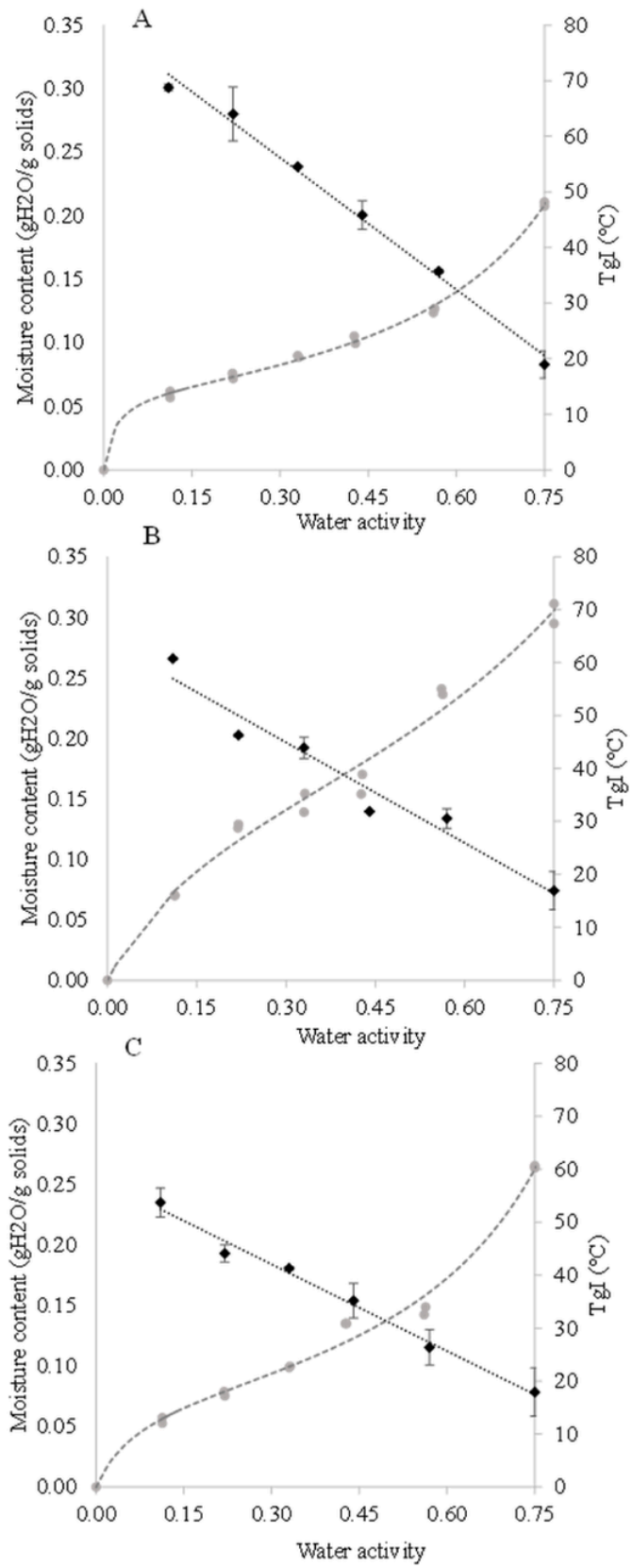

Fig. 4. Sorption isotherms and first glass transition (Tg_I) temperature as a function of water activity of films based on cassava starch (A), chitosan (B), and its blends (C). Lines in sorption isotherms and in glass transition temperature were calculated using the GAB model (Eq. (2)), and a linear equation (Table 3).

Table 1
Monolayer moisture content (X_m), C_{GAB}, and K_{GAB} parameters of GAB model, coefficients of determination (significance of coefficients $p < 0.05$), related Root Mean Square Error (RMSE), and mean relative percentage deviation (E).[a]

Films	X_m (%)	C_{GAB}	K_{GAB}	R^2	RMSE	E (%)
CS	6.2 (0.2)	58.3 (24.2)	0.94 (0.01)	0.997	0.00	2.79
CH	15.9 (2.7)	8.6 (2.7)	0.71 (0.08)	0.982	0.01	6.65
CS/CH	7.9 (0.7)	14.9 (6.7)	0.95 (0.03)	0.988	0.01	4.63

[a] CS: cassava starch, CH: chitosan, CS/CH: blend of cassava starch and chitosan. Values in brackets are standard errors.

K_{GAB} should be in between 0 and 1, and C_{GAB} should be higher than 0, as observed in this study (Table 1).

The entropic contribution can be well described by the K_{GAB}. K_{GAB} value of CS and the CS/CH blend films was near one, while CH film had a lower value of 0.71. The higher entropic content of K_{GAB} for films containing CS can be explained by the strongly increased number of configurations and mobility of water in the bulk liquid compared with the molecules in the multilayer. When K_{GAB} approaches one, there is almost no distinction between multilayer molecules and free liquid molecules. In that case, the water molecules beyond the monolayer are not structured in a multilayer but have the same characteristics as the molecules in the bulk liquid (and GAB→BET) (Blahovec and Yanniotis, 2008; Barbosa-Canovas et al., 2020).

Overall, the K_{GAB} values calculated in this study agrees with those calculated by several authors working on similar film compositions and temperature (Mali et al., 2005; Pelissari et al., 2011; Teodoro et al., 2015; Aguirre-Loredo et al., 2017; Monte et al., 2018). Moreover, some authors determined higher (Pelissari et al., 2011), lower (Mali et al., 2005; Aguirre-Loredo et al., 2017) and even similar (Mali et al., 2005; Monte et al., 2018) C_{GAB} values compared to those presented in Table 1.

3.2.5. *Differential scanning calorimetry (DSC)*

Water-macromolecule interactions change very rapidly in the vicinity of the Tg range (Lazaridou and Biliaderis, 2000). The temperature program with the selected annealing condition at 20 °C, allowed the detection of three Tg occurring at increasing temperatures, and one endothermal peak. According to Dong et al. (2004), DSC is not sensitive enough to detect the relaxation temperatures of polysaccharides, but after a convenient physical aging treatment of samples, these transitions in DSC thermograms became much more distinct because of the enthalpy relaxation.

Examples of DSC thermograms of the three films equilibrated at 22% RH at room temperature were shown in Fig. 5. After annealing, overall, three glass transitions were observed and called as Tg_I, Tg_{II} and Tg_{III} from the lower to higher temperature. Overall, the glass transition correspond to the α-relaxation and reflects motions of fairly long chain segments in the amorphous portion of biopolymer; other relaxation phenomena, including β-relaxation, are due to local movements of the main chain, or rotations and vibrations of terminal groups or of other side chains (Lazaridou and Biliaderis, 2000). In this work, it corresponds to Tg_I (Table 2).

All calculated Tg were presented in Table 2, where it was possible to observe the well-known plasticizer effect of water (Lazaridou and Biliaderis, 2000). With the increase of a_w, the respective X_w increased (Fig. 4), provoking a decrease in all Tg. For example, the CS film Tg_I decreased from 68.8 to 19 °C, the CH film Tg_{II} decreased from 157.5 to 138.8 °C, and the CS/CH blend film Tg_{III} decreased from 178.8 to 152.2 °C when the a_w increased from 0.11 to 0.75 (Table 2). As it is well known, films physical properties are strongly affected by Tg (Lazaridou and Biliaderis, 2000). For example, Bergo et al. (2008) observed that films based on CS became less stiff and rigid and more extendible due to Tg decrease.

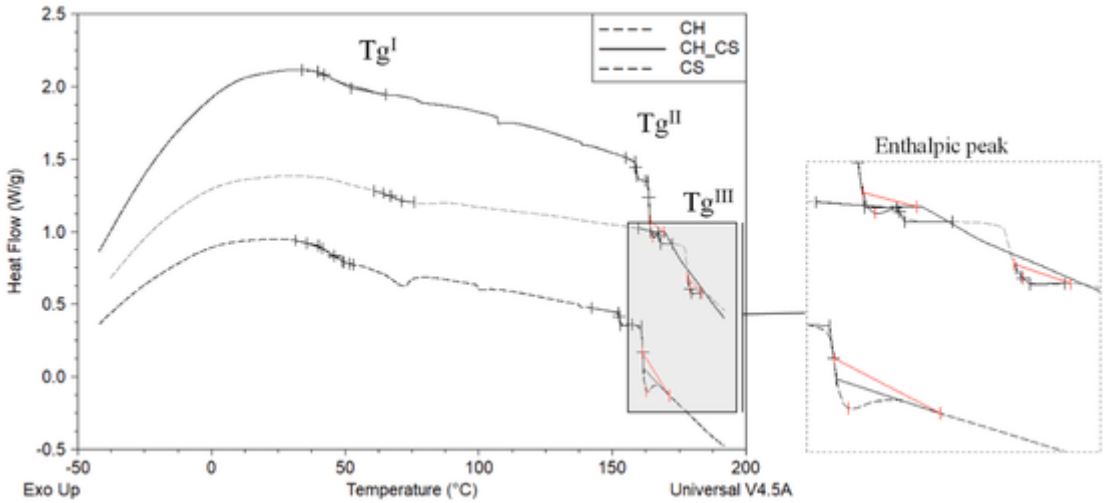

Fig. 5. Examples of DSC thermograms of films based on cassava starch (CS), chitosan (CH), and its blends (CS/CH) and conditioned at 0.22 of water activity.

Table 2
Glass transitions (Tg_I, Tg_{II}, Tg_{III}) and endothermal peak temperatures (°C) and enthalpy (ΔH, J/g).[a]

Films	a_w	Tg_I (ºC)		Tg_{II} (ºC)		Tg_{III} (ºC)		T peak (ºC)		ΔH peak (J/g)
CS	0.11	68.80	(0.55)	164.86	(0.14)	189.46	(1.31)	N.R. N.R.		
	0.22	64.02	(4.84)	164.97	(3.39)	182.62	(5.24)	175.55	(2.18)	0.53
	0.33	54.52	(0.20)	151.91	(2.19)	168.72	(0.71)	169.92	(1.33)	1.04
	0.44	45.83	(2.56)	145.39	(0.63)	162.12	(0.01)	168.48	(4.85)	1.26
	0.57	35.71	(0.33)	140.03	(3.25)	156.07	(4.38)	164.79	(0.07)	0.97
	0.75	18.95	(2.44)	137.78	(0.11)	155.87	(0.50)	157.58	(0.09)	1.37
CH	**0.11**	60.73	(0.18)	157.52	(1.56)	165.32	(2.47)	166.60	(2.55)	0.81
	0.22	46.29	(0.28)	153.02	(0.57)	161.29	(0.00)	162.59	(0.02)	0.54
	0.33	43.92	(2.01)	144.31	(2.09)	158.03	(2.56)	160.16	(0.70)	2.20
	0.44	31.88	(0.16)	139.24	(2.03)	148.65	(4.67)	157.06	(0.14)	0.86
	0.57	30.55	(1.85)	144.47	(6.36)	152.62	(0.44)	153.35	(0.46)	3.29
	0.75	16.91	(3.63)	139.77	(4.31)	149.85	(0.64)	152.18	(1.81)	1.83
CS/CH	**0.11**	53.72	(2.73)	163.35	(0.51)	178.65	(0.04)	178.83	(5.84)	1.23
	0.22	44.08	(1.62)	155.10	(3.36)	165.46	(2.03)	167.47	(3.12)	0.73
	0.33	41.28	(0.33)	148.09	(1.03)	164.68	(1.86)	165.90	(2.56)	2.55
	0.44	35.16	(3.26)	148.64	(2.83)	157.16	(1.33)	158.55	(1.56)	0.60
	0.57	26.37	(3.32)	141.09	(0.69)	155.25	(2.41)	158.36	(1.01)	1.16
	0.75	17.91	(4.56)	137.36	(1.02)	150.81	(1.67)	152.15	(1.80)	1.76

[a] CS: cassava starch, CH: chitosan, CS/CH: blend of cassava starch and chitosan. Values in brackets are standard errors.

The detection of multiple Tg by DSC analysis was previously reported in the literature on foods matrices (Iaccheri et al., 2020; Telis et al., 2006), but it is not usual on biopolymer films (López-Angulo et al., 2020). Famá et al. (2006) and Bergo et al. (2008), working on CS film, observed one Tg occurring in cryogenic temperature, which was associated to a glycerol rich fraction, and another one, above room temperature, which was associated to the biopolymer-rich fraction. But, Souza et al. (2012), also working on CS films, observed two Tg occurring at 36–39 and 57–63 °C, which are close to Tg_I (Table 2).

On the other side, Lazaridou and Biliaderis (2000) analyzed corn starch/CH films using a dynamical mechanical analyzer (DMA) and observed only one Tg for all films. Only one Tg was also observed by Bonilla et al. (2017) analysing CH films in a DSC. These authors determined Tg = 52 °C, which is in the range of Tg_I determined in this study (Table 2). Similarly, Dong et al. (2004) determined only one Tg on CH films after convenient annealing. Nevertheless, these authors analyzed CH films also by DMA and detected three events occurring at ~85, ~140 and ~197 °C, considerably higher than those determined in this study (Table 2). The first two phenomena were associated with α- and β-relaxation phenomena (Dong et al., 2004).

And finally, the endothermal peak, occurring just after Tg_{III} (Fig. 5), involving a very small enthalpy (Table 2), must be associated to an enthalpic relaxation phenomenon, probably related to an aging process of the amorphous glassy portion of film that absorbs energy to get back to an equilibrium state above Tg (Barbosa-Canovas et al., 2020).

Taking in consideration that it is critical for films physical properties and storage management (Chaudhary et al., 2011), Tg_I was considered for further discussions. So, in order to build a stability map for each film, Tg_I was plotted against a_w (Fig. 4), and a linear relationship was observed (Table 3). These stability maps can be useful for predicting Tg of films stored under various conditions, and to calculate the critical a_w value at 22 °C, that are 0.69 and 0.61 for CS, and CH and CS/CH blend films, respectively (Fig. 4), meaning that in this case, CH controlled this parameter. In food stored above this a_w critical value, some physical modifications such as loss of crispness, stickiness of powder, hard candies, recrystallization of amorphous sugars causing caking, mechanical modification including collapse phenomena, and loss of porosity as well as diffusion can occur (Labuza et al., 1972), and in biopolymeric films, changes in its mechanical properties can be expected, for instance. But, for active film, this parameter is important to the conservation of bioactive compounds into biopolymeric matrix. Films containing CH have a low critical a_w value compared to CS film. In this way, solid structures of CS film were more stable than that of CH containing films. This result agrees with the crystallinity study results (Fig. 3 D).

Table 3
Parameters ($p < 0.05$) of linear equations calculated by linear regression and coefficients of determination (level of confidence 95%), and related Root Mean Square Error (RMSE), and dielectric constant of monolayer (ε'_m).[a]

Films	*A*	*B*	R^2	RMSE	ε'_m
Tg = $Aa_w + B$					
CS	−79.2	79.9	0.993		–
CH	−63.4	64.0	0.954		–
CS/CH	−54.6	58.4	0.988		–
ε' = $AX_w + B$					
CS	0.33	1.90	0.975	0.25	1.17
CH	0.15	0.86	0.948	0.22	1.36
CS/CH	0.29	1.77	0.988	0.19	1.21

[a] CS: cassava starch, CH: chitosan, CS/CH: blend of cassava starch and chitosan. Tg: glass transition temperature (ºC), a_w: water activity, ε': dielectric constant, X_w: moisture content (d.b.).

Moreover, the Gordon & Taylor model (Eq. (2)) was applied to calculate the glass transition temperature (Tg_2) of the anhydro matrix of films, i.e., composed by biopolymer and glycerol (Habitante et al., 2008). According to this model, Tg decreases as a function of the plasticizer concentration increasing due to its effect on free volume of matrix (Chaudhary et al., 2011). The glass curves were showed in Fig. 6 for CS (in blue), CH (in orange) and CS/CH (in grey) films. Eq. (2) was fitted by non-linear regression to Tg_I *vs* moisture content (wet basis) data, using the Statistica® 7.0 (Stat-Soft Inc., USA), with good correlation coefficient ($R^2 \geq 0.92$) and RMSE (>3) (Table 4).

$$Tg_I = \frac{W_1 Tg_1 + W_2 k\, Tg_2}{W_1 + W_2 k} \quad (2)$$

where W_i and Tg_i are the mass fraction and glass transition temperatures of water ($i = 1$) and biolpolymer/glycerol matrix ($i = 2$), respectively, and k is the constant of Gordon & Taylor. Tg_2 and k were calculated by fitting, considering the water glass transition $Tg_1 = 138$ K (Habitante et al., 2008).

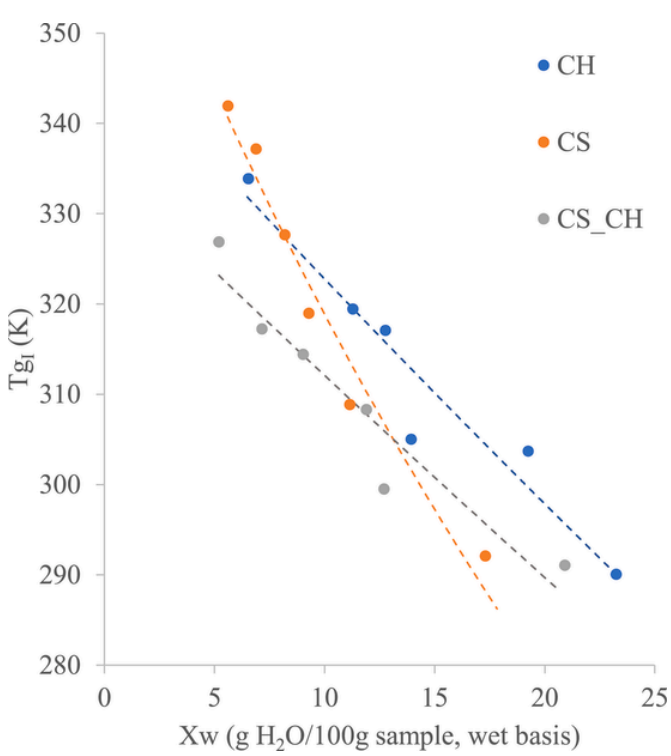

Fig. 6. Glass curves calculated by using the Gordon and Taylor model (Eq. (2)) for films based on cassava starch (CS), chitosan (CH), and its blends (CS/CH). Dots are experimental data.

Table 4
Gordon & Taylor model parameters (k and Tg_2) calculated by non-linear regression, and coefficients of determination, and related Root Mean Square Error (RMSE) (significance of coefficients $p < 0.05$).

Films	*k*	Tg_2 (K)	R^2	RMSE
CS	0.37 (0.05)	373.2 (6.8)	0.965	3.17
CH	0.78 (0.13)	349.1 (6.5)	0.928	3.72
CS/CH	0.83 (0.15)	335.4 (4.8)	0.917	3.40

*CS: cassava starch, CH: chitosan, CS/CH: blend of cassava starch and chitosan. Values in brackets are standard errors.

The k is related to a relation between the variation of heat capacity ($\Delta Cp_2/\Delta Cp_1$) of the components across transition from glassy to rubbery state (Habitante et al., 2008). As can be seen in Table 4, k of films containing CH ($k \approx 0.8$) was the twice of that for films based on CS ($k = 0.4$). This means that films based on CH and CS/CH blend presented a marked water plasticization effect. On the opposite trend, CS film was less sensible to water and for this, at low a_w it could suffer of fractures and brittleness due to its glassy/crystalline state, as reported on starch-based films (Ortega-Toro et al., 2017). This corroborates with the results on films crystallinity (Fig. 3D). Overall, the values of k calculated in this study were lower than those calculated by Chaudhary et al. (2011) working on starch plasticized by several plasticizer agents.

On another side, the value of Tg of the biopolymers/glycerol matrix, $Tg_2 = 100$, 75.9 and 62.2 °C (Table 4), were higher than $Tg_I = 68.8$, 53.7 and 60.7 °C related to the lower a_w (Table 2), for films based on CS, CS/CH and CH, respectively. Evidently, Tg_2 was higher because there was not water plasticizer effect in that condition. Nevertheless, these values were relatively low, for a medium molecular weight macromolecule, due to the presence of glycerol (20% in total).

The Gordon and Taylor model was also used to calculate the plasticizer effect of the glycerol on the biopolymer/glycerol matrix and for this it was necessary to know the glass transition temperature of glycerol, $Tg_1 = 180$ K (Habitante et al., 2008), and k value for the biopolymer/glycerol matrix. This was possible correcting the k values presented in Table 4 multiplying it by $\Delta Cp_{water}/\Delta Cp_{glycerol}$ (1.94 J/g.K/0.88 J/g.K) (Habitante et al., 2008). Then, the glass transition temperatures of pure biopolymers (Tg_{2bp}) films were calculated, $Tg_{2bp} = 159.3$, 99.1 and 84.8 °C for films based on CS, CS/CH and CH, respectively. The Tg_{2bp} of pure CS film was almost close to those determined by Chaudhary et al. (2011), 167 °C, and determined by Bergo et al. (2008), 132 °C, for films based on CS without plasticizer. The Tg_{2bp} of the pure CH film was lower than that determined by Dong et al. (2004), 140–150 °C, and by Sakurai et al. (2000), 203 °C, but slightly closer to that calculated by Lazaridou and Biliaderis (2000), 95 °C. These differences can be due to different molecular weights, among others causes.

3.2.6. *Dielectric properties*

Two domains were observed for the dielectric constant (ε′) behavior as a function of samples X_w (Fig. 7). In the domain until X_m, where water was bounded to active sites of biopolymer matrix, ε′ remained constant (ε'_m). Nevertheless, ε'_m (Table 3) increased linearly from 1.17 to 1.36 as a function of film X_m (Fig. 7, insert). Over X_m, ε′ increased linearly as a function of films X_w (Table 3). The dependence of ε′ on X_w was also directly linked to X_m but inversely (Fig. 7, insert). As expected, water contributes to dielectric properties behavior when it is not strongly bounded with the solid matrix. Water affects dielectric properties increasing polarization phenomena (Wang et al., 2009). In this way, the linear behavior above the X_m was related to water availability for polarization movement. Similar behavior was determined by Bergo et al. (2012), for films based on CS with different moisture content, observing that ε' was very low and constant for $X_w \approx X_m$, and that it increased lin-

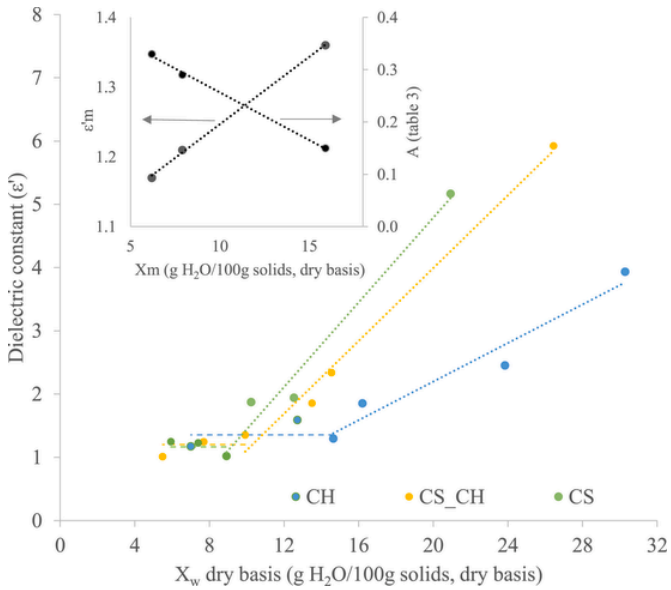

Fig. 7. Dielectric constant of films based on cassava starch (CS), chitosan (CH), and its blends (CS/CH) as a function of moisture content (X_w). Lines over X_m were calculated using the linear equation presented in Table 3. Insert shows the dielectric constant in the monolayer (ε'_m) and the slope of Equation presented in Table 3 as a function of the monolayer moisture content (X_m) of films. Lines were calculated by linear regression.

early for $X_w > X_m$, similarly to what observed in this study. These authors explained that in low a_w domain the water bound to the biopolymer structure contributed to low extent to the polarizability.

Considering that there is a strong interest on active film, the pitanga leave hydroethanolic extract (PLHE), rich in phenolic compounds, was added in the CS/CH films formulation, and analyzed for its dielectric properties. Thus, the incorporation of this PLHE into films allow to produce films with antioxidant and anti-microbial activities (Chakravartula et al., 2020), but affecting its gas barrier properties, as described at the end of section 3.2. The ϵ', ϵ" and σ of films based on passive CS, CH, and CS/CH and CS/CH with PLHE were shown in Fig. 8.

The decrease of ϵ' and ϵ" for all samples analyzed at high frequencies (Fig. 8) could be due to restrictions of ions polarization and molecular movement reduction (Abd El-Kader and Ragab, 2013). Fahmy et al. (2020) observed a similar behavior and attributed it to the building-up of a space charge layer at the sample-electrode interface. According to these authors, when the frequency of the applied field was increased, the polarization mechanism cannot obey the variation in the applied field and hence, the contribution of polarization to the ϵ' was reduced. Also, El Sayed and Mohamad (2018) observed similar behavior working on CH films in the same frequency range.

In the case of films based on CH, the two polar groups (-OH and $-NH_3^+$) (Hadi et al., 2020) were able to move under electromagnetic field at higher X_w of the analyzed films considering each a_w level. Despite these data, the dipolar rotations were limited, as the lowest ϵ' values describes. This confirm that not only the X_w or the chemical characteristic of a molecule determine the physical behavior, but also the state of the solid component, which can affect dielectric properties (Bergo et al., 2012, 2013).

CH film had the highest bound water content with less availability of water movement in the matrix described by sorption behavior. The water was bound to the matrix, and hence not free to move, more than CS film, which had a great crystalline part, and less total water holding capacity, but higher free water available for dipolar rotation. ϵ' and ϵ" of films based on blend of CS/CH revealed an additive effect hypothetically due to the interactions of the two components concentration increasing ion mobility.

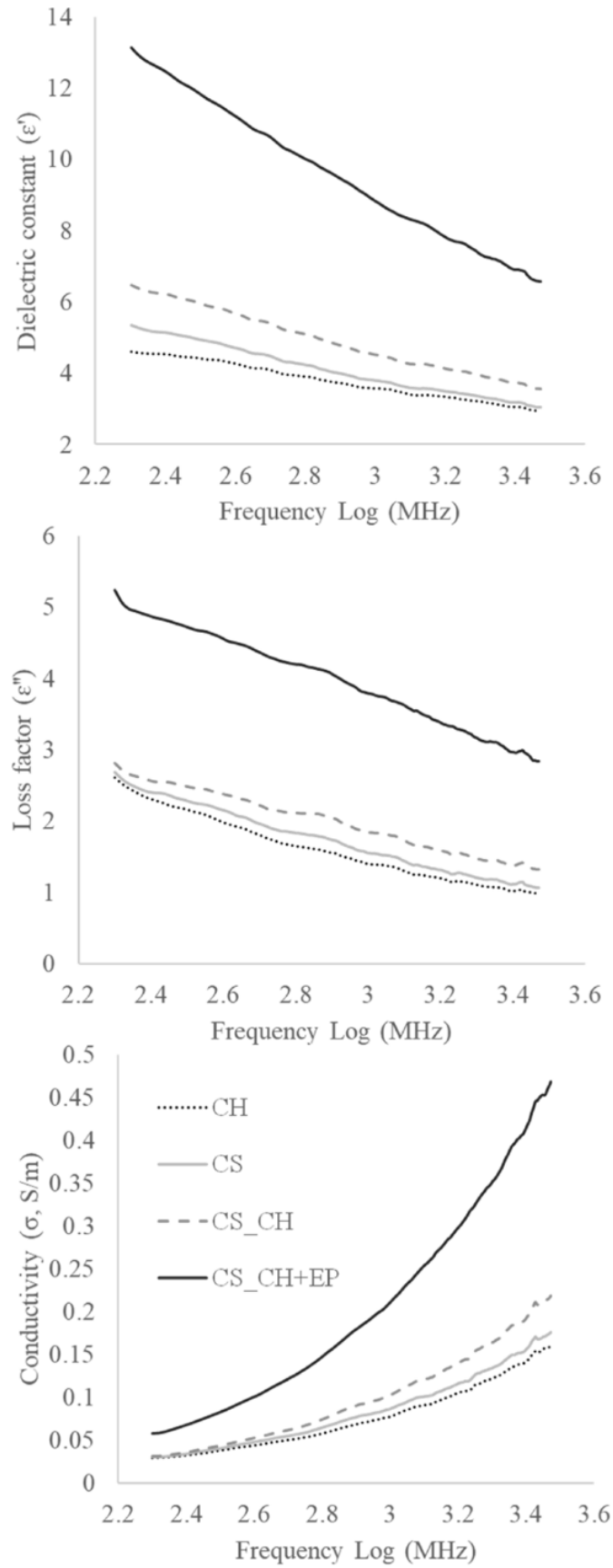

Fig. 8. Dielectric properties of films based on cassava starch (CS), chitosan (CH), and its blends (CS/CH), and of active films based on blends (CS/CH + PLHE) incorporated with pitanga leaves hydroethanolic extract (averaged data reported) as a function of frequency.

In a low-frequency region and above Tg, the dielectric properties of materials containing electrolytes and water are controlled by ionic conductivity (Iwamoto et al., 1999). The ϵ' is directly related to conductivity, and its increase will result in the increase number of charge carriers in the space charge accumulation region, and thus in the conductivity increase (Yusof et al., 2014). Furthermore, more amorphous portion is present in the material more ions mobility increase the stored charge in the electrolyte and consequently an increase of ϵ' and σ was observed (Yusof et al., 2014). However, the frequency range explored was not mainly related to conductivity, but to the dipolar rotation. Accordingly, σ revealed the same trend of ϵ', with the blend film showing the highest conductivity contribution, and the CH film the lowest.

The film based on CS/CH blend incorporated with PLHE presented a huge difference among all samples (Fig. 8). The molecular structure of phenolic compounds corresponds to a lower weight structure rich in hydroxyl groups and double links conjugated with single ones (Fennema, 1996), which contribute to increasing the side groups' movement and ionic charge available for energy accumulation and thus ϵ', ϵ" and σ, contributing to the increasing in gas permeability. In this way, the high ϵ', ϵ" and σ values for CS/CH films with PLHE, as observed in Fig. 8, should not be surprising. A high dielectric reactivity of phenolic compounds was previously reported by Hayat et al. (2010).

The absence of a clear peak in the dielectric spectra, which could be related to a relaxation phenomenon, was previously reported in literature for similar matrixes in the low frequency region (Hadi et al., 2020; Abd El-Kader and Ragab, 2013). However, the environmental temperature range presents a physical state modification reported by thermal properties, as Tg_I. As reported by Hadi et al. (2020), concerning low frequency range, relaxation peaks can be seen by plotting the complexity permittivity (ε_r), calculated by using Eq. (3), versus the Log frequency (Fig. 9).

$$\varepsilon_r = \sqrt{(\varepsilon'^2 + \varepsilon''^2)} \tag{3}$$

Fig. 9 show a clear visible peak imputable to α-relaxation for all the films analyzed. The trends of ε_r as a function of frequency was almost the same for all samples, nevertheless, an additive effect on ε_r of CS and CH on ε_r of CS/CH can be observed due to probably interactions between CS and CH which facilitated the polarization. Considering dielectric relaxation, a permanent dipole moment underwent as the main molecules process. Accordingly, blending CS and CH showed an additive effect due to the rise of ion availability and thus an increase in conductivity that contribute to dielectric response.

Dielectric constant of α-relaxation should be affected by a_w raise, as a direct consequence of a X_w increase. Furthermore, relaxation processes are related to the intra- and intermolecular interactions changes (Abd El-Kader and Ragab, 2013). Molecular rearrangement can be seen in the thermal properties exploiting a temperature modulation, and in the DS by the electromagnetic field that stimulates molecular motion as alignment or rotation of dipole involving in α-relaxation (Johari, 1976).

Afterward, the dielectric constant of α-relaxation (ε'_α) was calculated by an adaptation of the modified Gompertz model (Eq. (4)) (Traffano-Schiffo et al., 2017), and presented in Fig. 10. It is clear that different physical states, such as glassy, rubber or crystal can affect dielectric properties.

$$\varepsilon'_\alpha = 10^{\left(l\varepsilon'_\infty + \Delta l\varepsilon'_\gamma + \Delta l\varepsilon'_\beta + \frac{\Delta l\varepsilon'_\alpha}{2}\right)} \tag{4}$$

where: $l\Delta'_\infty$ is the logarithm of the dielectric constant at high frequencies, $\Delta l\Delta n'$ is the magnitude of each dispersion α, β, γ.

To further investigate this relation, an exponential model (Eq. (5)) relating α-relaxation (ε'_α) and the glass transition temperature (Tg_I in K) was proposed:

$$\varepsilon'_\alpha = \varepsilon'_{\alpha 0} e^{-k_\alpha Tg_I} \tag{5}$$

where $\varepsilon'_{\alpha 0}$ is the α-relaxation in the complete immobilization state ($Tg_I = 0$ K), and k_α is the α-relaxation rate constant (K^{-1}), calculated by non-linear regression (Table 5). It can be observed that α-relaxation decreased exponentially as a function of Tg_I, and apparently in parallel shift (Fig. 10). But, only apparently, because the parameters of Eq. (5) were quite differents (Table 5). Both parameters increased in the following order: CS < CH < CS/CH films (Table 5). Overall, the $\varepsilon'_{\alpha 0}$ values were very high ($\geq 10^9$) because at $Tg_I = 0$ K, both biopolymer, glyc-

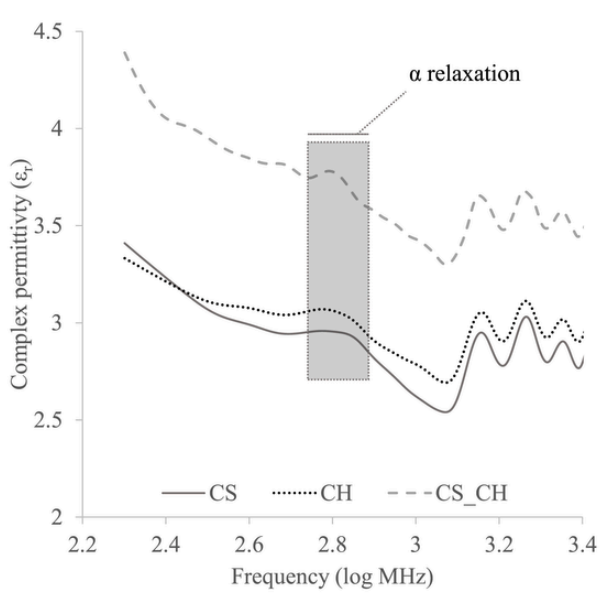

Fig. 9. Complex permittivity of films based on cassava starch (CS), chitosan (CH), and its blends (CS/CH), as a function of frequency (averaged spectra).

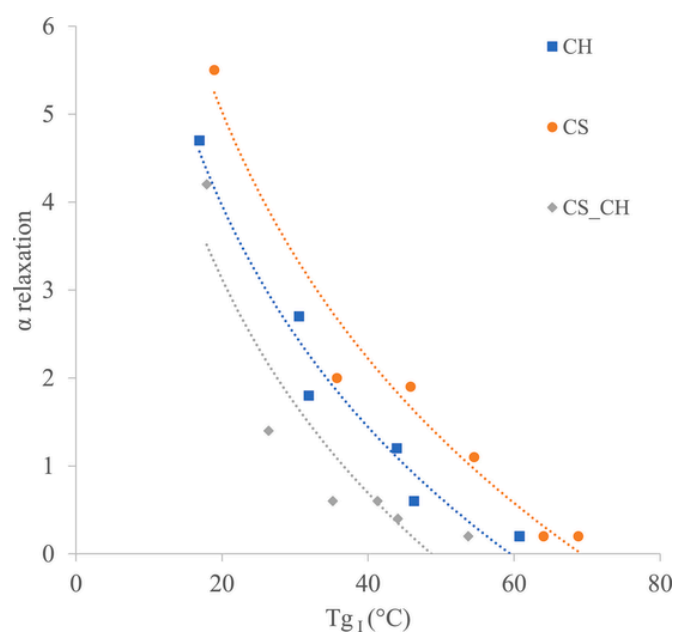

Fig. 10. Relation between α-relaxation and Tg_I of films based on cassava starch (CS), chitosan (CH), and its blends (CS/CH). Lines were calculated with Eq. (5).

Table 5
α-relaxation in the complete immobilization state ($\varepsilon'_{\alpha 0}$), and α-relaxation rate constant (k_α) calculated by non-linear regression using Eq. (5), and coefficients of determination, and related Root Mean Square Error (RMSE), (significance of coefficients $p < 0.05$).

Films	$\varepsilon'_{\alpha 0}$ (10^{-9})	k_α (10^2 K^{-1})	R^2	RMSE
CS	3	6.8	0.896	3.22
CH	8	7.2	0.952	0.67
CS/CH	50	8.1	0.960	0.22

*CS: cassava starch, CH: chitosan, CS/CH: blend of cassava starch and chitosan.

erol and water were completely immobilized, probably in a very low and constant free-volume state, making difficult the macromolecular relaxation. In other words, water and glycerol molecules lost their plasticizer effect, and then, the lower value of CS $\varepsilon'_{\alpha 0}$ can be explained by its higher crystallinity.

Moreover, the higher value of k_α of film based on CS/CH blend and the lower value for CS film means that these materials were more and less sensitive, respectively, to change of Tg. These results are in agreement to what observed for the Gordon and Taylor constant (Table 4). Therefore, a certain change in the Tg of materials should have a more important effect on dielectric properties of CS/CH blend film than CH film and CS film, similarly to the effect of the plasticizer concentration. Moreover, it is important to observe that the total amount of water including multilayer and free-water was higher for film based on CS/CH followed by CS and CH films, respectively. This amount of water means higher polarization under the effect of temperature and could probably influence others film physical properties. The immobilization of water molecules in the glass state reduces slightly the contribution to the dielectric properties (Lewicki, 2004). In order to better understand these results, furthers studies on β-relaxation and films physical aging must be carried out.

4. Conclusions

The physical state of water was accessed by the stability maps of CH, CS and CS/CH blend films which were made from sorption isotherm and T_{gI} data. The calculated parameters of GAB and related thermal properties were able to describe different film behaviours. CH film had lower water mobility than CS film. The blend film showed an intermediate behavior. On another side, the macromolecular physical state was verified by the thermal properties of films which resulted in three glass transition events due to several structures. In particular, Tg_I was near to the environmental temperature, so very important for the management of films storage. Molecular rearrangement producing Tg can be also observed by dielectric properties with α-relaxation for all film considered. Furthermore, the addition of phenolic compounds to activate the CS/CH film strongly influenced its dielectric properties, due to a molecular mobility increase.

All studied phenomena are linked. The moisture content varied as a function of water activity according to the GAB model, whereas Tg_I decreased linearly as a function of water activity and of moisture content following the Gordon and Taylor model; the dielectric constant increased linearly as a function of moisture content in a domain above the water monolayer, and α-relaxation was reduced exponentially as a function of Tg_I. All these related behaviors in the studied films were provoked by the changes in water-biopolymers and biopolymer-biopolymer interactions.

Funding

São Paulo State Research Foundation (FAPESP, Grant, 2013/07914–8). Brazilian National Council for Scientific and Technological Development (CNPq): Research fellowship of P.J.A.S (30.0799/2013–6) and grant (40.3746/2021–3). This study was financed in part by the "Coordenação de Aperfeiçoamento de Pessoal de Nível Superior – Brasil" (CAPES) - Finance Code 001 (Visiting Professor fellowship of P.J.A.S.) and by European Union, Horizon 2020 Programme, NewTechAqua Project, Grant Agreement No 862658.

Disclaiming

The views and opinions expressed in this publication are the sole responsibility of the author(s) and do not necessarily reflect the views of the European Commission/Research Executive Agency.

CRediT author statement

Eleonora Iaccheri: Conceptualization, Methodology, Investigation, Formal analysis, Writing- Original draft preparation; Valentina Siracusa: Methodology, Investigation, Writing- Reviewing and Editing. Luigi Ragni: Formal analysis, Writing- Reviewing and Editing; Ana Cristina A. S. Pinheiro: Investigation, Writing- Reviewing and Editing; Santina Romani: Writing- Reviewing and Editing; Pietro Rocculi: Writing- Reviewing and Editing; Marco Dalla Rosa: Supervision, Resources, Project administration, Writing- Reviewing and Editing. Paulo J. A. Sobral: Conceptualization, Methodology, Investigation, Validation, Writing- Original draft preparation Writing- Reviewing and Editing.

Declaration of competing interest

The authors declare the following financial interests/personal relationships which may be considered as potential competing interests: Paulo Jose do Amaral Sobral reports financial support was provided by University of Sao Paulo, Faculty of Animal Science and Food Engineering, Department of Food Engineering.

Data availability

Data will be made available on request.

References

Abd El-Kader, M.F.H., Ragab, H.S., 2013. DC conductivity and dielectric properties of maize starch/methylcellulose blend films. Ionics 19, 361–369. https://doi.org/10.1007/s11581-012-0742-8.

Aguirre-Loredo, R.Y., Rodriguez-Hernandez, A.I., Velazquez, G., 2017. Modelling the effect of temperature on the water sorption isotherms of chitosan films. Food Sci. Technol. 37 (1), 112–118. https://doi.org/10.1590/1678-457X.09416.

Barbosa-Canovas, G.V., Fontana, A.J., Schmidt, S.J., Labuza, T.P., 2020. Water Activity in Foods, second ed. IFT Press, Wiley Blackwell, ISBN 9781118768310.

Bergo, P.V.A., Carvalho, R.A., Sobral, P.J.A., Santos, R.M.C., Silva, F.B.R., Prison, J.M., Solorza-Feria, J., Habitante, A.M.Q.B., 2008. Physical properties of edible films based on cassava starch as affected by the plasticizer concentration. Packag. Technol. Sci. 21, 85–89. https://doi.org/10.1002/pts.781.

Bergo, P., Sobral, P.J.A., Prison, J.M., 2010. Effect of glycerol on physical properties of cassava starch films. J. Food Process. Preserv. 34, 401–410. https://doi.org/10.1111/j.1745-4549.2008.00282.x.

Bergo, P., Moraes, I.C.F., Sobral, P.J.A., 2012. Effects of moisture content on structural and dielectric properties of cassava starch films. Starch Staerke 64 (10), 835–839. https://doi.org/10.1002/star.201200023.

Bergo, P., Moraes, I.C.F., Sobral, P.J.A., 2013. Infrared spectroscopy, mechanical analysis, dielectric properties and microwave response of pigskin gelatin films plasticized with glycerol. Food Biosci. 1, 10–15. https://doi.org/10.1016/j.fbio.2013.01.001.

Blahovec, J., Yanniotis, S., 2008. GAB generalized equation for sorption phenomena. Food Bioprocess Technol. 1, 82–90. https://doi.org/10.1007/s11947-007-0012-3.

Bonilla, J., Sobral, P.J.A., 2016. Investigation of the physicochemical, antimicrobial and antioxidant properties of gelatin-chitosan edible film mixed with plant ethanolic extracts. Food Biosci. 16, 17–25. https://doi.org/10.1016/j.fbio.2016.07.003.

Bonilla, J., Bittante, A.M.Q.B., Sobral, P.J.A., 2017. Thermal analysis of gelatin-chitosan edible film mixed with plant ethanolic extracts. J. Therm. Anal. Calorim. 130, 1221–1227. https://doi.org/10.1007/s10973-017-6472-4.

Chakravartula, S.S.N., Lourenço, R.V., Balestra, F., Bittante, A.M.Q.B., Sobral, P.J.A., Dalla Rosa, M., 2020. Influence of pitanga (Eugenia uniflora L.) leaf extract and/or natamycin on properties of cassava starch/chitosan active films. Food Packag. Shelf Life 24, 100498. https://doi.org/10.1016/j.fpsl.2020.100498.

Chaudhary, D.S., Adhikari, B.P., Kasapis, S., 2011. Glass-transition behaviour of plasticized starch biopolymer system - a modified Gordon-Taylor approach. Food

Hydrocolloids 25 (1), 114–121. https://doi.org/10.1016/j.foodhyd.2010.06.002.
Dong, Y., Ruan, Y., Wang, H., Zhao, Y., Bi, D., 2004. Studies on glass transition temperature of chitosan with four techniques. J. Appl. Polym. Sci. 93, 1553–1558. https://doi.org/10.1002/app.20630.
Duran-Baron, R., Luquez, L., Mejia, J., Perez, L., Sobral, P.J.A., 2017. Production and characterization of films based on blends of chitosan from blue crab (*Callinectes sapidus*) waste and pectin from Orange (*Citrus sinensis* Osbeck) peel. Int. J. Biol. Macromol. 98, 676–683. https://doi.org/10.1016/j.ijbiomac.2017.02.004.
El Sayed, A.M., Mohamad, A.D.M., 2018. Synthesis, structural, thermal, optical and dielectric properties of chitosan biopolymer; influence of PVP and α-Fe2O3 Nanorods. J. Polym. Res. 25, 175. https://doi.org/10.1007/s10965-018-1571-x.
Fahmy, T., El Hendawi, H., El Sharkawy, W.B., Reicha, F.M., 2020. AC conductivity and dielectric relaxation of chitosan/poly(vinyl alcohol) biopolymer polyblend. Bull. Mater. Sci. 43, 243. https://doi.org/10.1007/s12034-020-02207-2.
Famá, L., Flores, S.K., Gerschenson, L., Goyanes, S., 2006. Physical characterization of cassava starch biofilms with special reference to dynamic mechanical properties at low temperatures. Carbohydr. Polym. 66, 8–15. https://doi.org/10.1016/j.carbpol.2006.02.016.
Fennema, O.R., 1996. Food Chemistry, third ed. CRC Press, ISBN 0-8247-9691-8.
Habitante, A.M.B.Q., Sobral, P.J.A., Carvalho, R.A., Solorza-Feria, J., Bergo, P.V.A., 2008. Phase transitions of cassava starch dispersions prepared with glycerol solutions. J. Therm. Anal. Calorim. 93 (2), 599–604. https://doi.org/10.1007/s10973-007-8950-6.
Hadi, J.M., Aziz, S.B., Nofal, M.M., Hussein, S.A., Hafiz, M.H., Brza, M.A., Abdulwahid, R.T., Kadir, M.F.Z., Woo, H.J., 2020. Electrical, dielectric property and electrochemical performances of plasticized silver ion-conducting chitosan-based polymer nanocomposites. Membranes 10, 151. https://doi.org/10.3390/membranes10070151.
Hayat, K., Zhang, X., Chen, H., Xia, S., Jia, C., Zhong, F., 2010. Liberation and separation of phenolic compounds from citrus Mandarin peels by microwave heating and its effect on antioxidant activity. Separ. Purif. Technol. 73, 371–376. https://doi.org/10.1016/j.seppur.2010.04.026.
Iaccheri, E., Castagnini, J.M., Dalla Rosa, M., Rocculi, P., 2020. New insights into the glass transition of dried fruits and vegetables and the effect of pulsed electric field treatment. Innovat. Food Sci. Emerg. Technol. 67, 102566. https://doi.org/10.1016/j.ifset.2020.102566.
Iwamoto, S., Kumagai, H., Hayashi, Y., Miyawaki, O., 1999. Conductance and relaxations of gelatin films in glassy and rubbery states. Int. J. Biol. Macromol. 26 (5), 345–351. https://doi.org/10.1016/S0141-8130(99)00105-1.
Johari, G.P., 1976. Glass transition and secondary relaxations in molecular liquids and crystal. Ann. N. Y. Acad. Sci. 279 (1), 117–140. https://doi.org/10.1111/j.1749-6632.1976.tb39701.x.
Labuza, T.P., McNally, L., Gallagher, D., Hawkes, J., Hurtado, F., 1972. Stability of intermediate moisture foods. J. Food Sci. 37, 154–159. https://doi.org/10.1111/j.1365-2621.1972.tb03408.x.
Lazaridou, A., Biliaderis, C.G., 2000. Thermophysical properties of chitosan. Chitosan starch and chitosan–pullulan films near the glass transition. Carbohydr. Polym. 48, 179–190. https://doi.org/10.1016/S0144-8617(01)00261-2.
Lertsutthiwong, P., Noomun, K., Khunthon, S., Limpanart, S., 2012. Influence of chitosan characteristics on the properties of biopolymeric chitosan-montmorillonite. Prog. Nat. Sci.: Mater. Int. 22 (5), 502–508. https://doi.org/10.1016/j.pnsc.2012.07.008.
Lewicki, P.P., 2004. Water as the determinant of food engineering properties. A review. J. Food Eng. 61 (4), 483–495. https://doi.org/10.1016/S0260-8774(03)00219-X.
López-Angulo, D.E., Bittante, A.M.Q.B., Luciano, C.G., Valencia, G.A., Flaker, C.H.C., Djabourov, M., Sobral, P.J.A., 2020. Effect of Laponite® on the structure, thermal stability and barrier properties of nanocomposite gelatin films. Food Biosci. 35, 100596. https://doi.org/10.1016/j.fbio.2020.100596.
Lorenzo, J.M., Vargas, F.C., Strozzi, I., Pateiro, M., Furtado, M.M., Sant'Ana, A.S., Roccheti, G., Barba, F.J., Dominguez, R., Lucini, L., Sobral, P.J.A., 2018. Influence of pitanga leaf extracts on lipid and protein oxidation of pork burger during shelf-life. Food Res. Int. 114, 47–54. https://doi.org/10.1016/j.foodres.2018.07.046.
Mali, S., Sakanaka, L.S., Yamashita, F., Grossmann, M.V.E., 2005. Water sorption and mechanical properties of cassava starch films and their relation to plasticizing effect. Carbohydr. Polym. 60, 283–289. https://doi.org/10.1016/j.carbpol.2005.01.003.
Monte, M.L., Moreno, M.L., Senna, J., Arrieche, L.S., Pinto, L.A.A., 2018. Moisture sorption isotherms of chitosan-glycerol films: thermodynamic properties and microstructure. Food Biosci. 22, 170–177. https://doi.org/10.1016/j.fbio.2018.02.004.
Ortega-Toro, R., Collazo-Bigliardi, S., Rosello, J., Santamarina, P., Chiralt, A., 2017. Antifungal starch-based edible films containing Aloe vera. Food Hydrocolloids 72, 1–10. https://doi.org/10.1016/j.foodhyd.2017.05.023.
Pavia, D.L., Lampman, G.M., Kriz, G.S., 2001. Introduction to spectroscopy, third ed. Thomson Learning, London.
Pelissari, F.M., Yamashita, F., Grossmann, M.V.E., 2011. Extrusion parameters related to starch/chitosan active films properties. Int. J. Food Sci. Technol. 46, 702–710. https://doi.org/10.1111/j.1365-2621.2010.02533.x.
Pelissari, F.M., Andrade-Mahecha, M.M., Sobral, P.J.A., Menegalli, F.C., 2013. Comparative study on the properties of flour and starch films of plantain bananas (Musa paradisiaca). Food Hydrocolloids 30, 681–690. https://doi.org/10.1016/j.foodhyd.2012.08.007.
Sakurai, K., Maegawa, T., Takahashi, T., 2000. Glass transition temperature of chitosan and miscibility of chitosan/poly(N-vinyl pyrrolidone) blends. Polymer 41, 7051–7056. https://doi.org/10.1016/S0032-3861(00)00067-7.
Silva-Weiss, A., Bifani, V., Ihl, M., Sobral, P.J.A., Gómez-Guillén, M.C., 2013. Structural properties of films and rheology of film-forming solutions based on chitosan and chitosan-starch blend enriched with murta leaf extract. Food Hydrocolloids 31, 458–466. https://doi.org/10.1016/j.foodhyd.2012.11.028.
Siracusa, V., 2012. Food packaging permeability behaviour: a report. Int. J. Polym. Sci. 302029. https://doi.org/10.1155/2012/302029. . 2012. .
Siracusa, V., Romani, S., Gigli, M., Mannozzi, C., Cecchini, J.P., Tylewicz, U., Lotti, N., 2018. Characterization of active edible films based on citral essential oil, alginate and pectin. Materials 11. https://doi.org/10.3390/ma11101980. . 1980. .
Souza, A.C., Benze, R., Ferrão, E.S., Ditchfield, C., Coelho, A.C.V., Tadini, C.C., 2012. Cassava starch biodegradable films: influence of glycerol and clay nanoparticles content on tensile and barrier properties and glass transition temperature. LWT - Food Sci. Technol. (Lebensmittel-Wissenschaft -Technol.) 46, 110–117. https://doi.org/10.1016/j.lwt.2011.10.018.
Tapia-Blácido, D.R., Sobral, P.J.A., Menegalli, F.C., 2013. Effect of drying conditions and plasticizer type on some physical and mechanical properties of amaranth flour films. LWT - Food Sci. Technol. (Lebensmittel-Wissenschaft -Technol.) 50 (2), 392–400. https://doi.org/10.1016/j.lwt.2012.09.008.
Telis, V.R.N., Sobral, P.J.A., Telis-Romero, J., 2006. Sorption isotherm, glass transitions and state diagram for freeze-dried plum skin and pulp. Food Sci. Technol. Int. 12, 181–187. https://doi.org/10.1177/1082013206065953.
Teodoro, A.P., Mali, S., Romero, N., Carvalho, G.M., 2015. Cassava starch films containing acetylated starch nanoparticles as reinforcement: physical and mechanical characterization. Carbohydr. Polym. 126, 9–16. https://doi.org/10.1016/j.carbpol.2015.03.021.
Tessaro, L., Luciano, C.G., Bittante, A.M.Q.B., Lourenço, R.V., Martelli-Tosi, M., Sobral, P.J.A., 2021. Gelatin and/or chitosan-based films activated with "Pitanga" (Eugenia uniflora L.) leaf hydroethanolic extract encapsulated in double emulsion. Food Hydrocolloids 113, e106523. https://doi.org/10.1016/j.foodhyd.2020.106523.
Traffano-Schiffo, M.V., Castro-Giraldez, M., Colom, R.J., Fito, P.J., 2017. Development of a spectrophotometric system to detect white striping physiopathy in whole chicken carcasses. Sensors 17 (5), 1024. https://doi.org/10.3390/s17051024.
Valencia, G., Henao, A.C.A., Zapata, R.A.V., 2014. Influence of glycerol content on the electrical properties of potato starch films. Starch - Stärke 66, 260–266. https://doi.org/10.1002/star.201300038.
Valencia, G.A., Djabourov, M., Sobral, P.J.A., 2016. Water desorption of cassava starch granules: a study based on thermogravimetric analysis of aqueous suspensions and humid powders. Carbohydr. Polym. 147, 533–541. https://doi.org/10.1016/j.carbpol.2016.04.030.
Valencia, G.A., Luciano, C.G., Lourenço, R.V., Sobral, P.J.A., 2018. Microstructure and physical properties of nano-biocomposite films based on cassava starch and laponite. Int. J. Biol. Macromol. 107, 1576–1583. https://doi.org/10.1016/j.ijbiomac.2017.10.031.
Vicentini, N.M., Dupuy, N., Leitzelman, M., Cereda, M.P., Sobral, P.J.A., 2005. Prediction of cassava starch edible film properties by chemometric analysis of infrared spectra. Spectrosc. Lett. 38, 749–753. https://doi.org/10.1080/00387010500316080.
Wang, Y., Tang, J., Wang, Y., Swanson, B., 2009. Dielectric properties of eggs whites and whole eggs as influenced by thermal treatments. LWT--Food Sci. Technol. 42, 1204–1212. https://doi.org/10.1016/j.lwt.2009.02.018.
Wiles, J.L., Vergano, P.J., Barron, F.H., Bunn, J.M., Testin, R.F., 2000. Water vapor transmission rates and sorption behavior of chitosan films. J. Food Sci. 65 (7), 1175–1179. https://doi.org/10.1111/j.1365-2621.2000.tb10261.x.
Yusof, Y.M., Majid, N.A., Kasmani, R.M., Illias, H.A., Kadir, M.F.Z., 2014. The effect of plasticization on conductivity and other properties of starch/chitosan blend biopolymer electrolyte incorporated with ammonium iodide. Mol. Cryst. Liq. Cryst. 603 (1), 73–88. https://doi.org/10.1080/15421406.2014.966261.